Idaho Incubation Fund Program

Final Report Form

Proposal No.	**IF 14 004**
Name:	**Maria Mitkova**
Name of Institution:	**Boise State University**
Project Title:	**Research on Films with Columnar Structure to Improve Memristors Speed, Reliability and Lifespan**
	July 1, 2013 – June 31, 2014

Information to be reported in your final report is as follows:

1. Provide a summary of overall project accomplishments to include goals/milestones met, any barriers encountered, and how the barriers were overcome:

In this project we worked on formation of columnar structures within the Ge_xSe_{1-x} (x = 20%, 30%, 40%) chalcogenide glasses and extended its application to Redox Conductive Bridge Memory (RCBM). The Ge-Se films were deposited under oblique angles by thermally evaporation method. Holding the sample surface at an oblique angle to the arriving vapor flux resulted in a columnar morphology within the Ge-Se chalcogenide matrix, which aided in improving the device performance by controlling the filament growth through these nanostructures.
Study of the bare films provided insight into the obliquely deposited films average surface roughness and structural changes occurring in the layers by changing deposition temperature or deposition angle. These investigations were performed using Scanning Electron Microscopy, Atomic Force Microscopy (AFM), Energy Dispersive X-ray Spectroscopy (EDS) and Raman Spectroscopy. After studying bare columnar structure films, RCBM devices having columnar structure with the chalcogenide films were fabricated at Idaho Microfabrication Laboratory at Boise State University. The devices were electrically characterized by conducting current vs. voltage (IV) measurements, Read/Write voltage, the two resistive states, switching rate, and the reliability.

The material and electrical characterization results of the obliquely deposited bare films and the RCBM devices with nano-columnar structures are presented in the following section.

Material Research Related to Columnar Structures

Since a combination of factors, including the vapor directions, surface diffusion of the arriving vapor on the substrate, properties of the material being deposited, kinetic energy of the arriving vapor, and vacuum pressure plays a role in the formation of columnar structures. Therefore, simple geometry rules such as tangent and cosine laws do not apply to the obliquely deposited films for predicting the columnar structures growth. The most important step of the research work was to establish the conditions under which the columnar structures films could be grown. Based on the experimental results performed in this research, we proposed an empirical formula, equation 1, to predict the growth the growth of the Ge-Se columnar structures.

$$\tan\alpha = \frac{2}{A}\tan\beta \qquad (1)$$

where A is a parameter that depends on materials and deposition rate, α is the incident vapor flux (deposition angle) and β is the columnar growth angle. The parameter A for the chalcogenide glasses studied in this work was found to be 0.625.

Cross-Sectional Study of Obliquely Deposited ChG Films

The cross-sectional SEM images of Ge_xSe_{1-x} (x = 0.2, 0.3, 0.4) and Ge_xTe_{1-x} (x = 0.2, 0.5) films deposited at different vapor incident angles (α = 90°, 60°, and 45°) are shown in Figure 1 and Figure 2, respectively. Inspection of these images illustrate that films deposited under oblique angles are composed of columns and inter-columnar voids. These voids provide directional pathways for the silver filament to grow. The obliquely deposited films are inclined towards the direction of the incoming vapor flux. The average column width, in of Ge-Se and Ge-Te films, were found to be ~19.13nm and ~22.56nm with an average spacing of ~15.64nm and ~18.45nm between the columns, respectively. This highly oriented nano columnar structure fabricated by obliquely deposited films is anisotropic in nature.

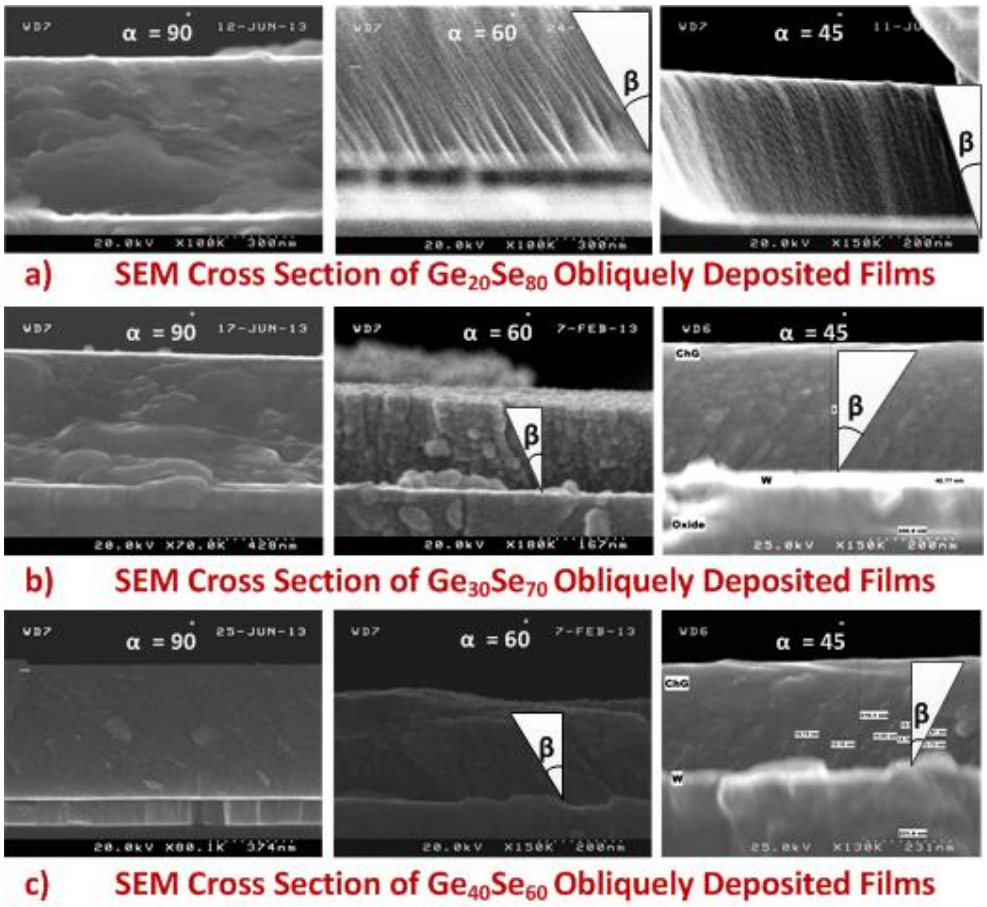

Figure 1 **SEM cross-sectional images of (a) $Ge_{20}Se_{80}$, (b) $Ge_{30}Se_{70}$, and (c) $Ge_{40}Se_{60}$ under various incident vapor angles: (i) α = 90°, (ii) α = 60°, (iii) α = 45°**

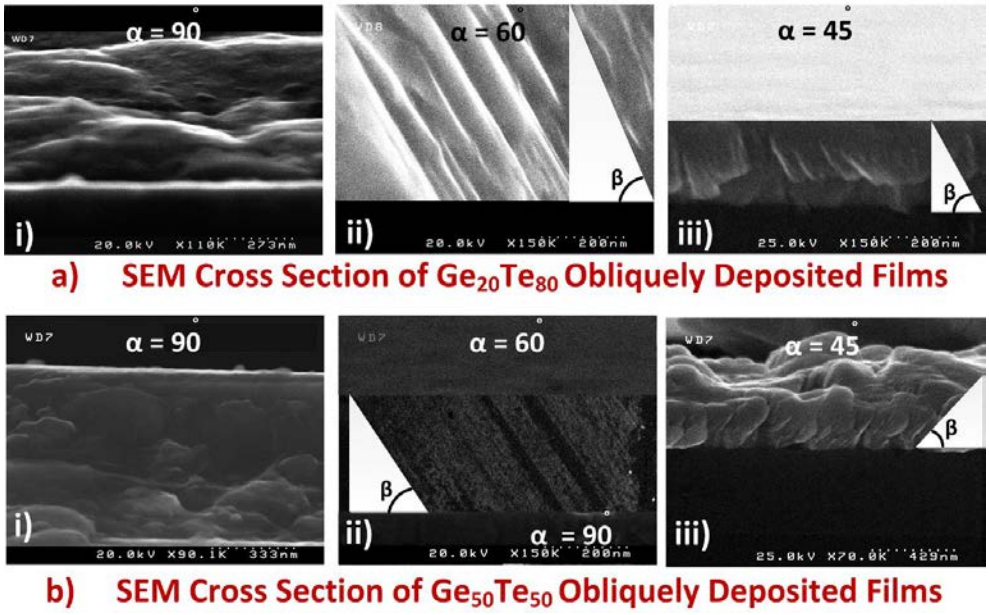

Figure 2 **SEM cross-sectional images of (a) $Ge_{20}Te_{80}$ and (b) $Ge_{50}Te_{50}$ under various incident vapor angles: (i) α = 90°, (ii) α = 60°, (iii) α = 45°**

Surface Morphology of Obliquely Deposited Films

Even though SEM is a good technique for characterizing thin films, it has limitations in characterizing the chalcogenide films, which are sensitive towards the interaction with the electron beam that results in collapsing of the column structure. Because of this, surface morphologies of the obliquely deposited films were also studied by AFM in tapping mode.

AFM surface scans, on a 500nm by 500nm area, for the obliquely deposited Ge-Se and Ge-Te films are presented in Figure 3 and Figure 4, which illustrate that the obliquely deposited films are predominantly porous in nature. The normally deposited films, in both Ge-Se and Ge-Te, have relatively smooth surface. A close observation of the AFM height bar scale, z-axis, indicates that the voids start to get larger and larger as the deposition angle decreases, which leads to a conclusion that the inter-columnar spacing increases at steeper angles.

In addition to studying the surface morphologies with AFM, the cross-sectional topography of the columnar structures were also studied using AFM. The SEM results for the columnar structures growth in the Ge-Se system with deposition angles of 60° and 45°, and Ge-Te films with deposition angles of 45° were validated by AFM. The inclination of the columnar structures towards the vapor flux in both the systems, are obvious from Figure 5 and Figure 6.

Since with decreasing the deposition angle the voids start to grow bigger, the surface roughness will be the smallest for the normally deposited films and will gradually increase as the deposition angle becomes smaller. This was confirmed by analyzing the surface roughness of the obliquely deposited films over a 5μm x 5μm area on both the Ge-Se and Ge-Te chalcogenide glasses and the results are presented in Figure 7 and Figure 8, respectively.

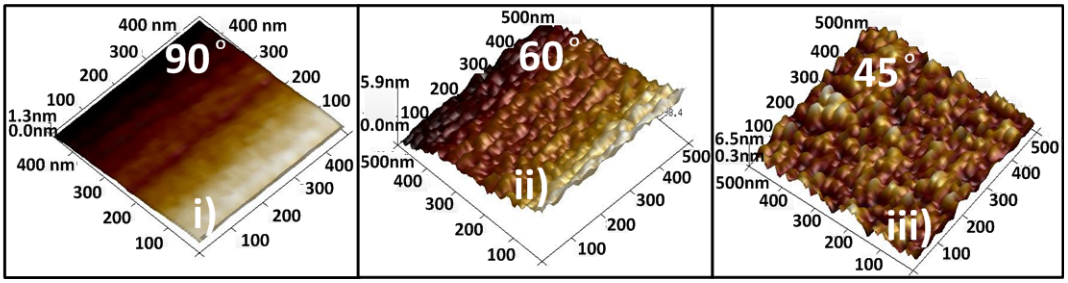

a) Angular deposition of $Ge_{20}Se_{80}$ films

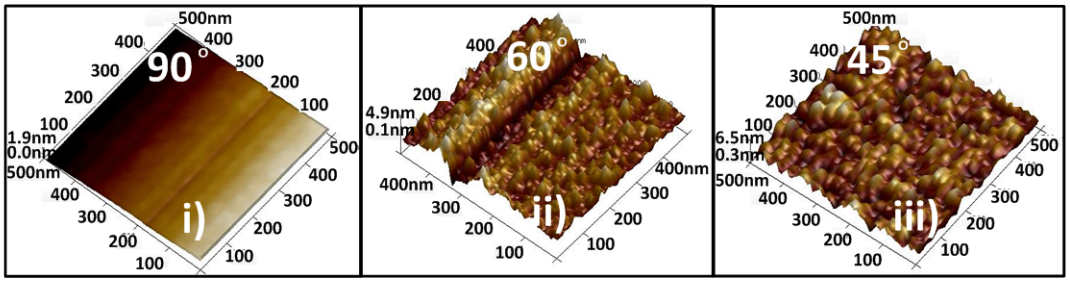

b) Angular deposition of $Ge_{30}Se_{70}$ films

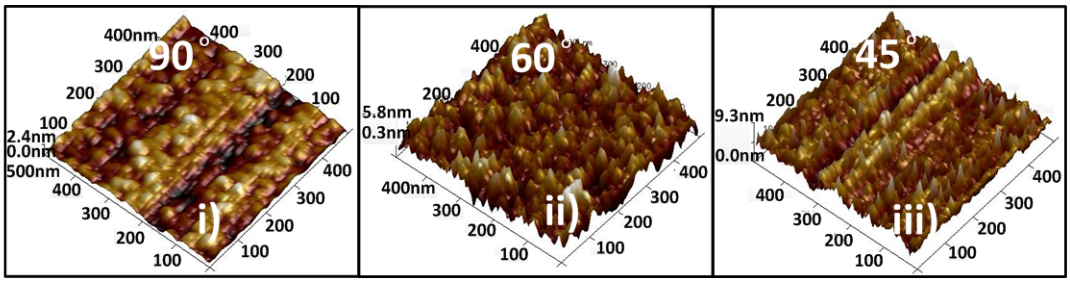

c) Angular deposition of $Ge_{40}Se_{60}$ films

Figure 3 AFM images for obliquely deposited (a) $Ge_{20}Se_{80}$, (b) $Ge_{30}Se_{70}$, and (c) $Ge_{40}Se_{60}$ films under various angles: (i) α = 90°, (ii) α = 60°, (iii) α = 45°

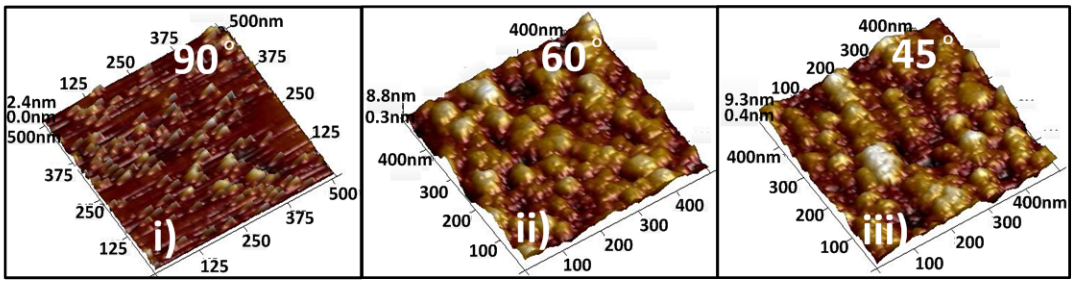

a) Angular deposition of $Ge_{20}Te_{80}$ films

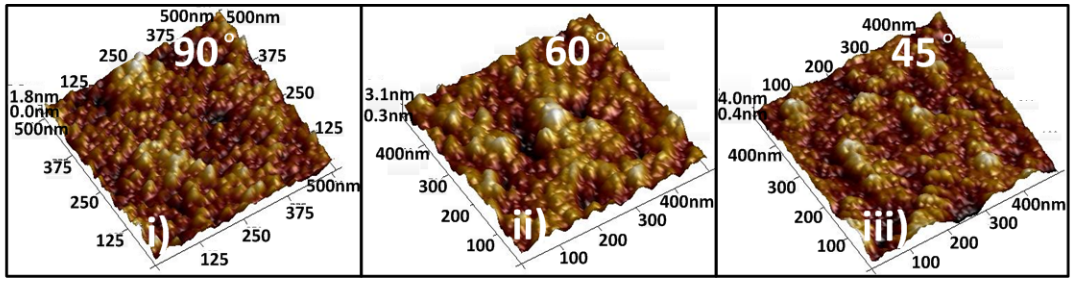

b) Angular deposition of $Ge_{50}Te_{50}$ films

Figure 4 AFM images for obliquely deposited (a) $Ge_{20}Te_{80}$ and (b) $Ge_{50}Te_{50}$ films under various angles: (i) α = 90°, (ii) α = 60°, (iii) α = 45°

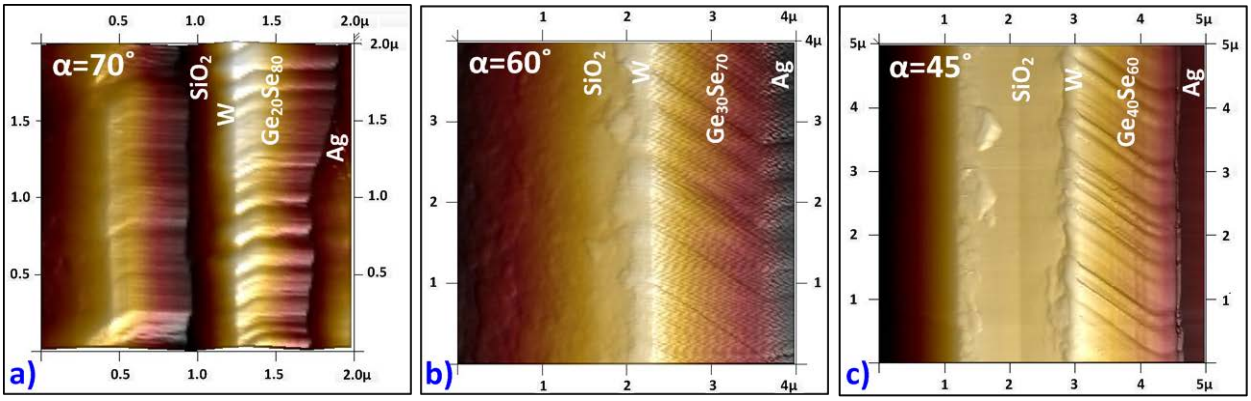

Figure 5 AFM images of the columnar structure by scanning on the sample cross-section of (a) $Ge_{20}Se_{80}$ at α = 70°, (b) $Ge_{30}Se_{70}$ at α = 45°, and (c) $Ge_{40}Se_{60}$ at α = 30°

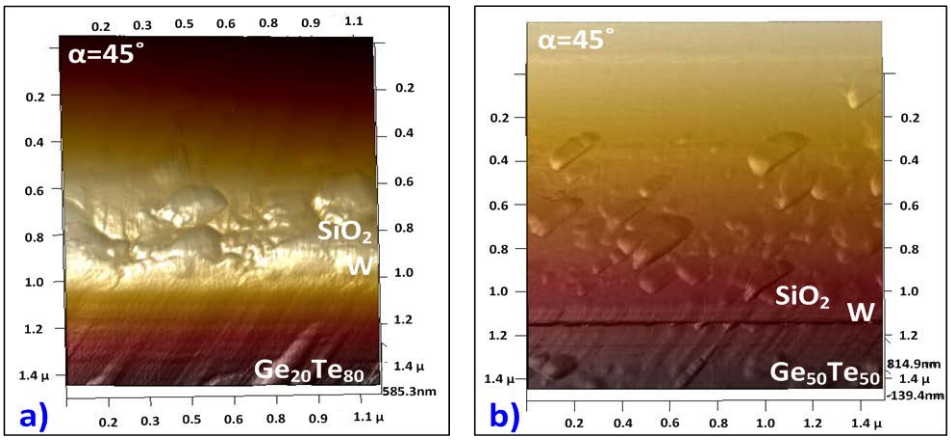

Figure 6 AFM images of the columnar structure by scanning on the sample cross-section of (a) $Ge_{20}Te_{80}$ at α = 45° and (b) $Ge_{50}Te_{50}$ at α = 45°

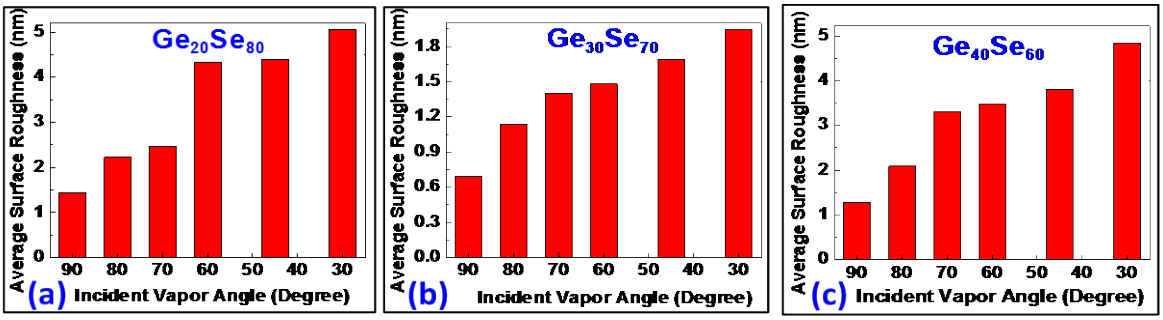

Figure 7 Average surface roughness observed in (a) Ge20Se80, (b) Ge30Se70, and (c) Ge40Se60 films under different depositions angles

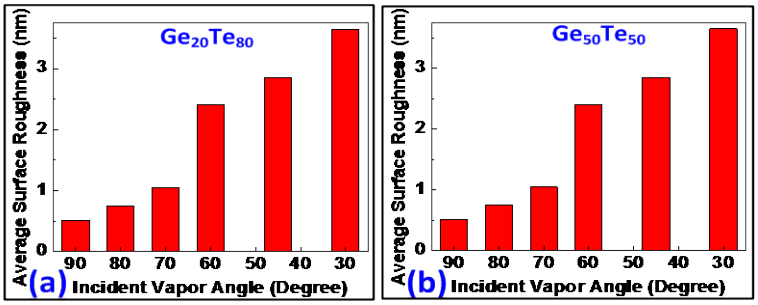

Figure 8 Average surface roughness observed in (a) Ge20Te80 and (b) Ge50Te50 films under various deposition angles

Compositional Analysis of Obliquely Deposited Films

Since the device performance is dependent on the composition, it was important to study the compositional variations caused by altering the incident vapor angle. Investigation of Ge-Se films compositions as a function of vapor incident angle is presented in Figure 9a. The composition of the normally evaporated films (α = 90°) is equal to the source composition for the $Ge_{30}Se_{70}$ and $Ge_{40}Se_{60}$ while the Se richest films with source composition $Ge_{20}Se_{80}$ was Se depleted as the normally deposited films contained 75 at% Se. For $Ge_{40}Se_{60}$ composition, the Se concentration decreased with the decrease in incident vapor flux angle, whereas for the other two compositions, an opposite trend was observed; that is, the Se concentration increased as the incident vapor flux arrived the substrate under lower angle. In the Ge-Te films, Figure 9b, a decreasing trend is observed for $Ge_{50}Te_{50}$ composition. However, no specific trend is observed in $Ge_{20}Te_{80}$.

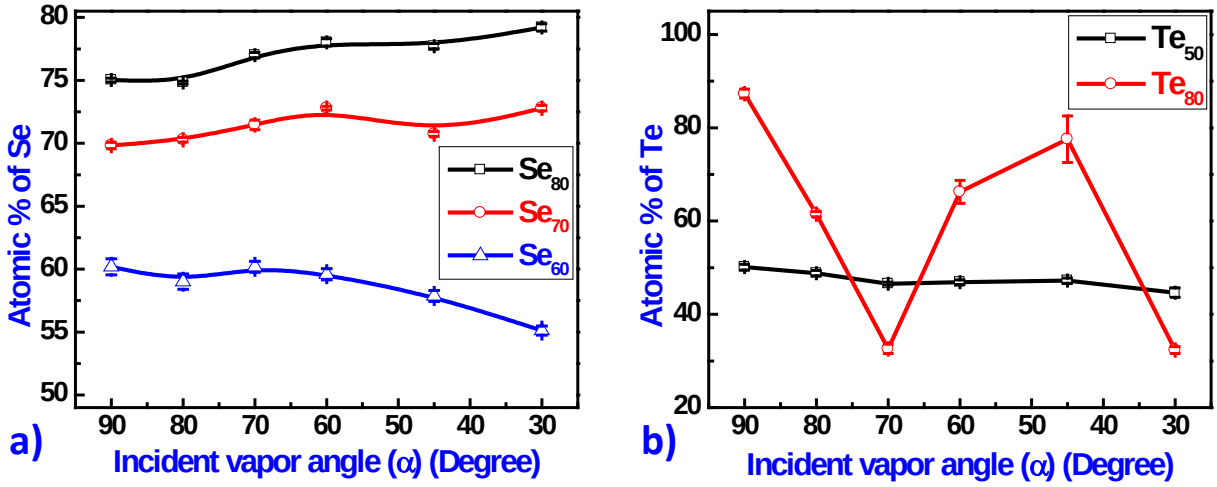

Figure 9 **Compositional analysis of (a) Ge_xSe_{1-x} (x = 0.2, 0.3, 0.4) and (b) Ge_xTe_{1-x} (x = 0.2, 0.5) films by altering the vapor flux angles**

The normally evaporated films (α = 90°) are usually the standard for evaluating the evaporation technique. The results for $Ge_{30}Se_{70}$ and $Ge_{40}Se_{60}$ films in Figure 9a support the choice of crucible (shaped in the form of Semi-Knudsen cell) and the evaporation rate since their compositions correspond to the source material. The Se rich samples resulted in Ge richer films, which is related to the high partial pressure of Se that contributes to repulsion of some Se atoms reaching the substrate with high energy. Evaporation of the Se rich compositions under oblique angles increased the Se content since, in these cases, the Se atoms reach the surface under a glancing angle, which reduces the energy of the interaction with the substrate and so reduces the repulsion of the Se atoms. The slight decrease of the Se content from the Ge rich films in the process of oblique deposition could be related to the full structural reorganization of these films, discussed in the Raman analysis section.

Raman Analysis of Obliquely Deposited Films

The Raman spectra of the obliquely deposited Ge-Se and Ge-Te films provided insight into the structural changes occurring in each film as a function of the

vapor flux angle. The major result from these studies is that although the films had well expressed morphology, they were amorphous in their nature.

Raman spectra for $Ge_{20}Se_{80}$, $Ge_{30}Se_{70}$, and $Ge_{40}Se_{60}$ obliquely deposited films are depicted in Figure 10. In general, three regions in these spectra are distinguishable: (i) a relatively sharp high intensity band around 197cm^{-1} along with a shoulder lobe around 214cm^{-1}, (ii) a high intensity and broad spanning 225 to 300 cm^{-1}, and (iii) a low intensity band ranging from 305 to 330cm^{-1}. In the 1st region, the 197cm^{-1} band corresponds to symmetric stretching of Se atoms in Ge-Se-Ge linkages that are corner shared (CS) between $GeSe_4$ tetrahedra while the 214cm^{-1} band corresponds to the breathing mode of a pair of Se atoms that are edge sharing (ES) two neighboring $GeSe_4$ tetrahedra. The frequency band in the 2nd region corresponds to the Raman characteristic spectrum of pure Se and is related to Se-Se stretching in Se chains and rings. The last band is due to an asymmetric vibration in the $GeSe_4$ edge shared tetrahedral. In addition, the spectra of $Ge_{30}Se_{70}$ and $Ge_{40}Se_{60}$ reveal a sharp but low intensity band centered at ~178 cm^{-1}, which originates from Ge–Ge homopolar bond related to the ethane-like structure (ETH). Also, in these two compositions, the band in 2nd region at 263cm^{-1} shifts to higher wavenumbers with increasing Ge content and, in the $Ge_{40}Se_{60}$ film, both the initially resolved bands in the 3rd region (~263 and ~310cm^{-1}) merge into a broad and intense band for films deposited under very low obliquely angle.

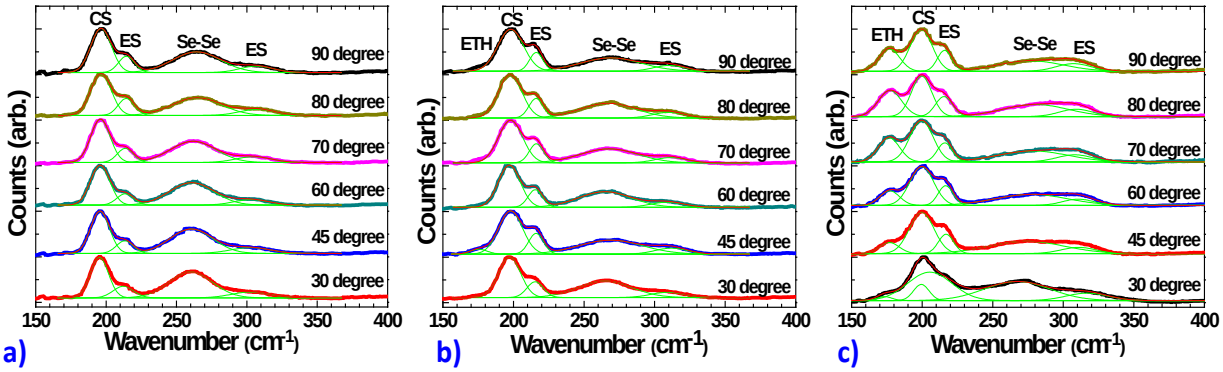

Figure 10 **Raman Spectra for obliquely deposited (a) $Ge_{20}Se_{80}$, (b) $Ge_{30}Se_{70}$, and (c) $Ge_{40}Se_{60}$ films under different angles**

The compositional results could be related to the structure of the films with the aid of Raman Spectroscopy studies. Raman spectra of $Ge_{20}Se_{80}$ films show a clear red shift in CS frequency mode, characteristic for increased Se concentration illustrated in the EDS data, with decreasing the deposition angle as shown in Figure 11a. This property is accompanied with an increase of the areal intensity of the Se-Se band vibration as shown in Figure 12a. The intensity of the vibrations for the CS mode increases in $Ge_{20}Se_{80}$, which suggests that the structure relaxes by enhancement of its floppiness due to the formation of a three-dimensional network built predominantly by CS Ge-Se tetrahedra. This is indeed a structure that resembles the structure of the $Ge_{20}Se_{80}$ bulk glass.

The structural data for the $Ge_{30}Se_{70}$ films are ambiguous as the frequency mode of the CS undergoes variations, which are not in a clear dependence of the deposition angle. At the same time, the Se-Se areal intensity as well as the amount of Se in these films increases as a function of decreasing deposition

angle, Figure 12a. There is not a clear dependence of these compositional changes related to changes of the areal intensity of the ES/CS structural units, Figure 12b. This suggest that, at this particular case, a phase separation occurs that keeps the equilibrium between the three dimensional Ge containing structural units with the Se-Se chains and rings.

The structural development for the Ge rich samples has an interesting development as a function of deposition angle. The packing stress is obviously released by destruction of the ETH structural units, which contributes to dense structural organization, which is relieved by formation of a tetrahedral structure with much bigger molecular volume. The stress release is the main reason for the structural reorganization as the angle decreases. A question may arise, what is building the column structures and how the structures are separated in the Ge-Se system? It is suggested that the columns are built by three-dimensional structural units containing Ge-Se tetrahedra connected in the inter-column space with Se-Se bonds.

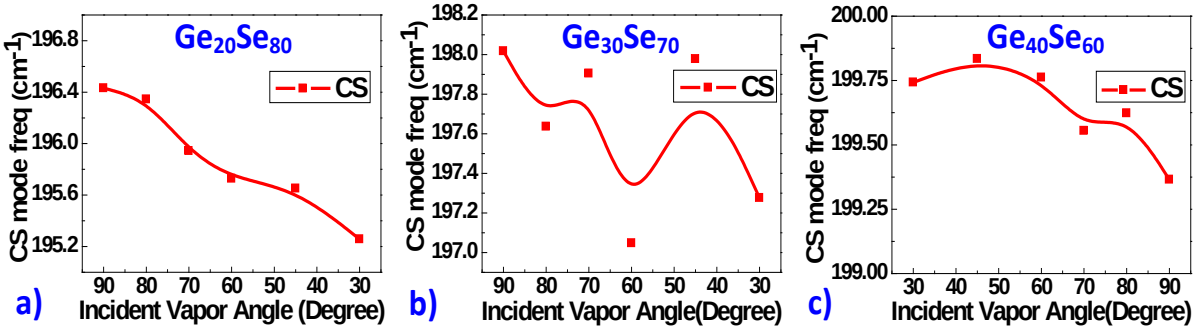

Figure 11 **Variations in CS-mode as a function of obliqueness angle in (a) $Ge_{20}Se_{80}$, (b) $Ge_{30}Se_{70}$, and (c) $Ge_{40}Se_{60}$ films**

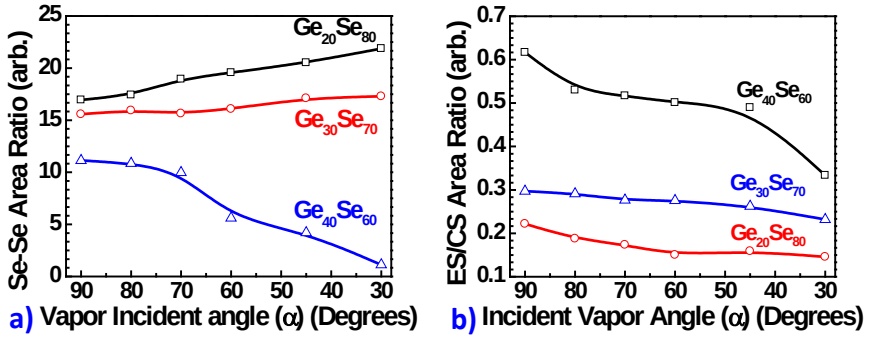

Figure 12 **Raman intensity area ratio of (a) Se-Se and (b) ES/CS bonding for Ge-Se system as a function of obliqueness angle**

The Raman spectra for $Ge_{20}Te_{80}$ and $Ge_{50}Te_{50}$ are presented in Figure 13. In both films compositions, there are three primary bands located at $88cm^{-1}$, $127cm^{-1}$, and $162cm^{-1}$ corresponding to rocksalt, corner-shared structure, and edge-shared structures, respectively. The other bands that are present at $95cm^{-1}$ and $118cm^{-1}$ correspond to the rocksalt and the corner shared structures. The aforementioned list of band locations, which have been ascribed in the fitted Raman results, are accepted as the primary bands for Ge-Te chalcogenide glass system. However, in $Ge_{20}Te_{80}$, films another peak arises at $150cm^{-1}$, which is attributed to the Te-Te bonding and is derived from the study of a-Te and c-Te

material. The Raman spectra for a-Te reveals a peak at 150cm^{-1}, while the crystalline phase produces a band at 123cm^{-1}, therefore it can be concluded that $Ge_{20}Te_{80}$ films are amorphous in nature due to the presence of this specific peak and shape without steep tops.

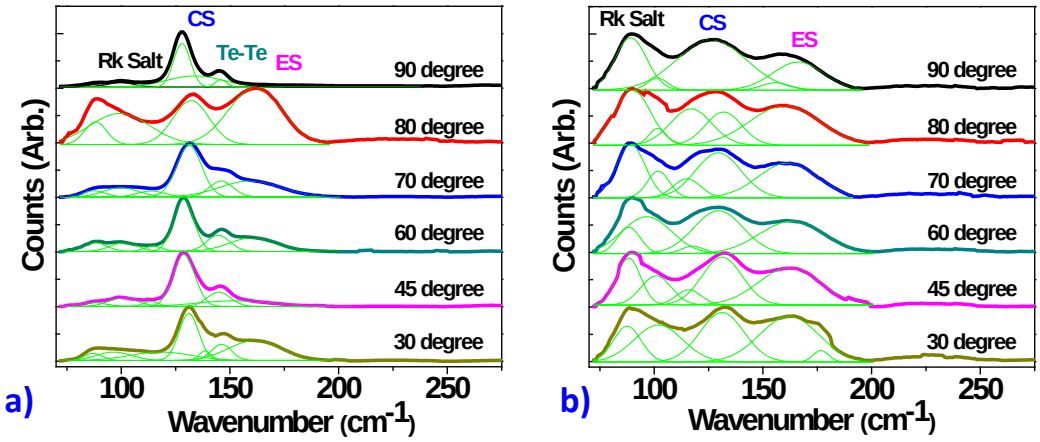

Figure 13 **Raman Spectra for obliquely deposited (a) $Ge_{20}Te_{80}$ and (b) $Ge_{50}Te_{50}$ films**

In contrast to Ge-Se films, the deconvoluted Raman spectra in terms of the vibrational mode frequency, for the Te rich and Ge rich films, reveal structural changes occurring in the films as a function of altering deposition angle. A large shift is observed in CS mode (and of course others modes as well) as illustrated in Figure 14.

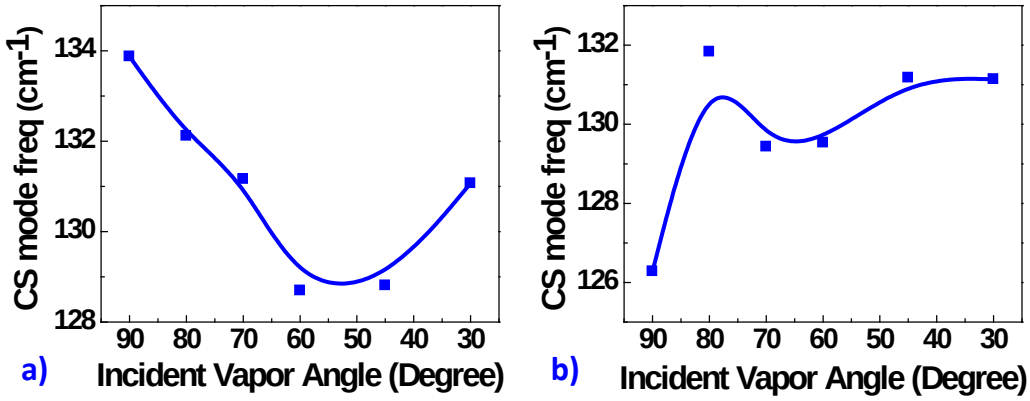

Figure 14 **Variations in CS-mode as a function of obliqueness angle in (a) $Ge_{20}Te_{80}$ and (b) $Ge_{50}Te_{50}$**

The structural changes are better understood by plotting the area ratios of the corresponding modes, which are presented in Figure 15. Figure 15a illustrates a decrease in the ES/CS structural units in Te rich samples with no significant changes in the Ge rich samples (Figure15b). The Te rich films at $\alpha = 90^{\circ}$ reveal no ES bonding, resulting in no data point for the ES/CS ratio in Figure15a. The Te containing glasses offer a unique ability to analyze the rocksalt structure. In both Ge-Te compositions, a decrease in rocksalt bonding is observed by decreasing the deposition angle, with the Ge rich sample undergoing a larger change as illustrated in Figure 15b. Also, the homopolar bonding in Te rich films is observed to be less dominant in the normally deposited films. However, an increase in Te-Te bonding can be noticed in Figure 4.36a by decreasing the

bonding angle. In the Ge rich films, no homopolar bonding is detected, as expected.

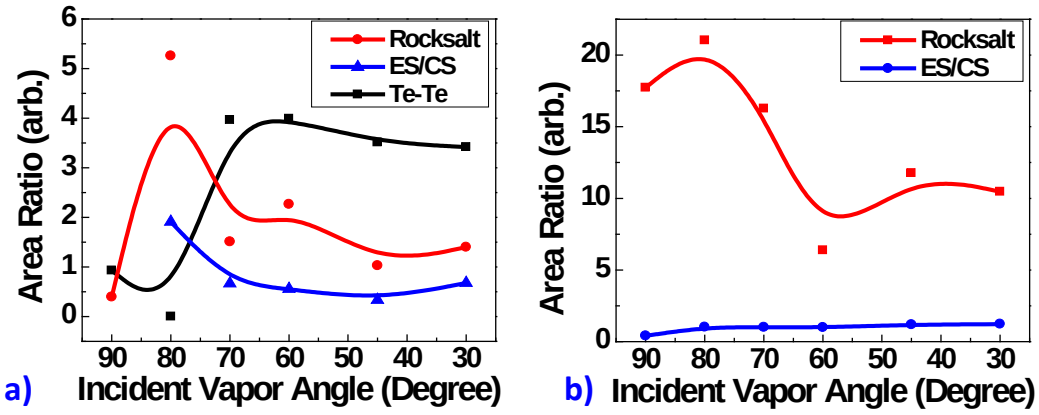

Figure 15 **Area ratio illustrating various bonds trends in (a) $Ge_{20}Te_{80}$ and (b) $Ge_{50}Te_{50}$ as a function of obliqueness angles**

The observed changes in the rocksalt layered structure reveal that there is a structural transition after α = 80°, in both systems. Prior to this transition, the rise of the rocksalt is attributed to the local rearrangement of the structure and the beginning of the columnar formation. The columns that are formed at α = 80° can be due to the specific structure of the rocksalt units with a ternary coordinated Ge and Te. The further structural reorganization with decreasing of the deposition angle suggests the occurrence of phase separation with similar composition specifics as in the system with Se, characterized by columns formed by tetrahedral structural units and inter-columnar space filled with Te chains.

Electrical Testing Of Fabricated Devices with Columnar Structures

Aside from the process technology for developing the nano-columnar structures in Ge-Se and Ge-Te chalcogenide glasses, the backbone of this work was to reflect the improvement achieved in the fabricated devices with the formation of columnar structures in RCBM devices. The RCBM devices were fabricated at Idaho Microfabrication Laboratory (IML) at Boise State University (BSU). Several electrical characterizations were performed on both the Ge-Se and Ge-Te fabricated devices by us as illustrated in the following section:

Endurance Measurements

The emerging resistive memories are targeting Flash applications, which require these devices to have an endurance of well over 10^4 switching cycles. The endurance measurements, for the fabricated RCBM devices, were carried out with Agilent 4155B Semiconductors Parameter Analyzer equipped with triax cables to avoid residual charge buildup. The IV characteristics of the Ge-Se and Ge-Te devices with films deposited normally (α = 90°) and obliquely (α = 45° and 60°) are presented in Figure 16 and Figure 17, respectively. The improvement in the device switching voltage variation is obvious for the devices having columnar structures.

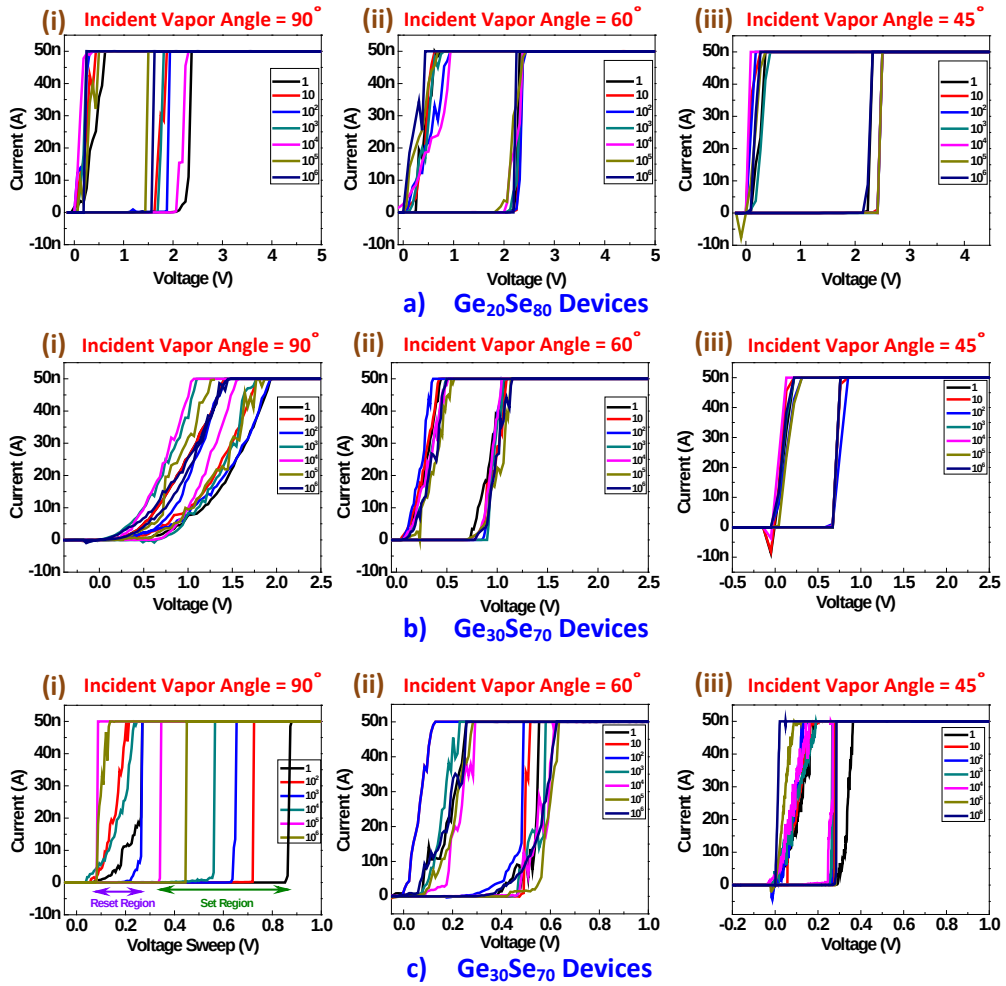

Figure 16 **IV curves for 10^6 cycles for Ge-Se devices having nano-columnar structure in the active films that are deposited under various incident angles: (i) α = 90°, (ii) α = 60°, (iii) α = 45°**

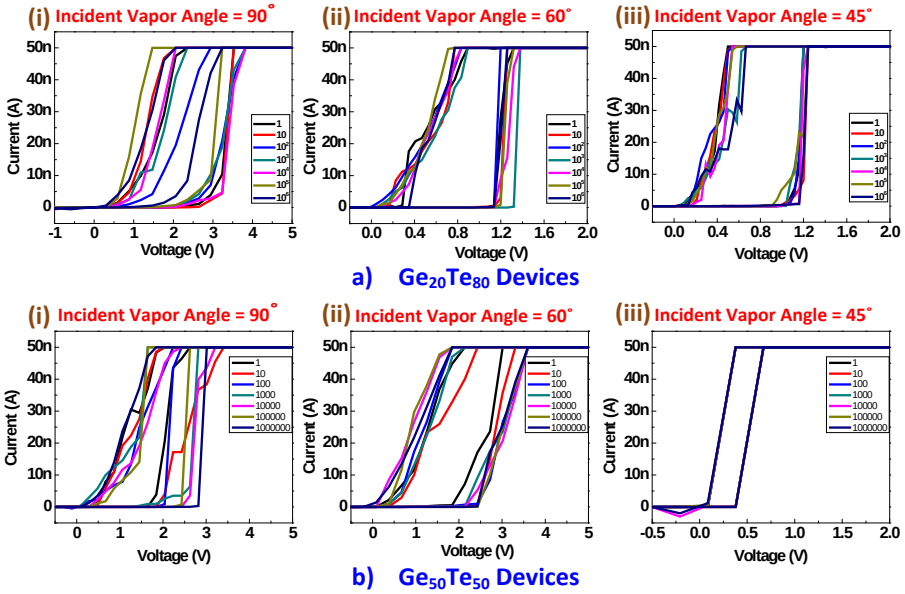

Figure 17 **IV curves for 10^6 cycles for Ge-Te devices having nano-columnar structure in the active films that are deposited under various incident angles: (i) α = 90°, (ii) α = 60°, (iii) α = 45°**

Another improvement achieved with the nano-structured devices is the shift of programming threshold voltage to relatively higher voltages. Hence, the probability of devices', embedded into the integrated circuit, falsely switching during an event of noise generation will be minimal. The higher switching voltage is attributed to the longer distance the ions have to travel for the formation of the filament and the reduction of the effective area taking part in the redox reaction. To accumulate the charge Q_o, the ion current $(I = jA_{eff})$, has to be effective for a certain programming time, $t_{prog.}$ This relation can be expressed as:

$$t_{prog} = \frac{Q_o}{j\ A_{eff}}$$

Since with the formation of columnar structures in the devices active layer, the effective area, A_{eff}, participating in the silver ions generation is reduced, thus the time to program (write) the RCBM devices increase, resulting in higher SET voltage of the device.

Memory Window

Memory window, for RCBM devices, is defined as the resistance difference between the ON and OFF states of the device. Mathematically, it can be expressed as:

$$Memory\ Window = R_{OFF} - R_{ON}$$

Having a good memory window will ensure a larger tolerance value for the read out bit stored in the RCBM cell, thus reducing the circuit complexity of the error correction bit.

In the column structured devices, no deterioration has been observed in the memory window. The fabricated devices show four to five orders of magnitude difference between the HRS and LRS as illustrated in the resistance-voltage (RV) plot in Figure 18 (Ge-Se system) and Figure 19 (Ge-Te System), respectively. The consistency in the switching voltage is also presented on the plot to highlight the improvement achieved in the devices by formation of such nano-structures.

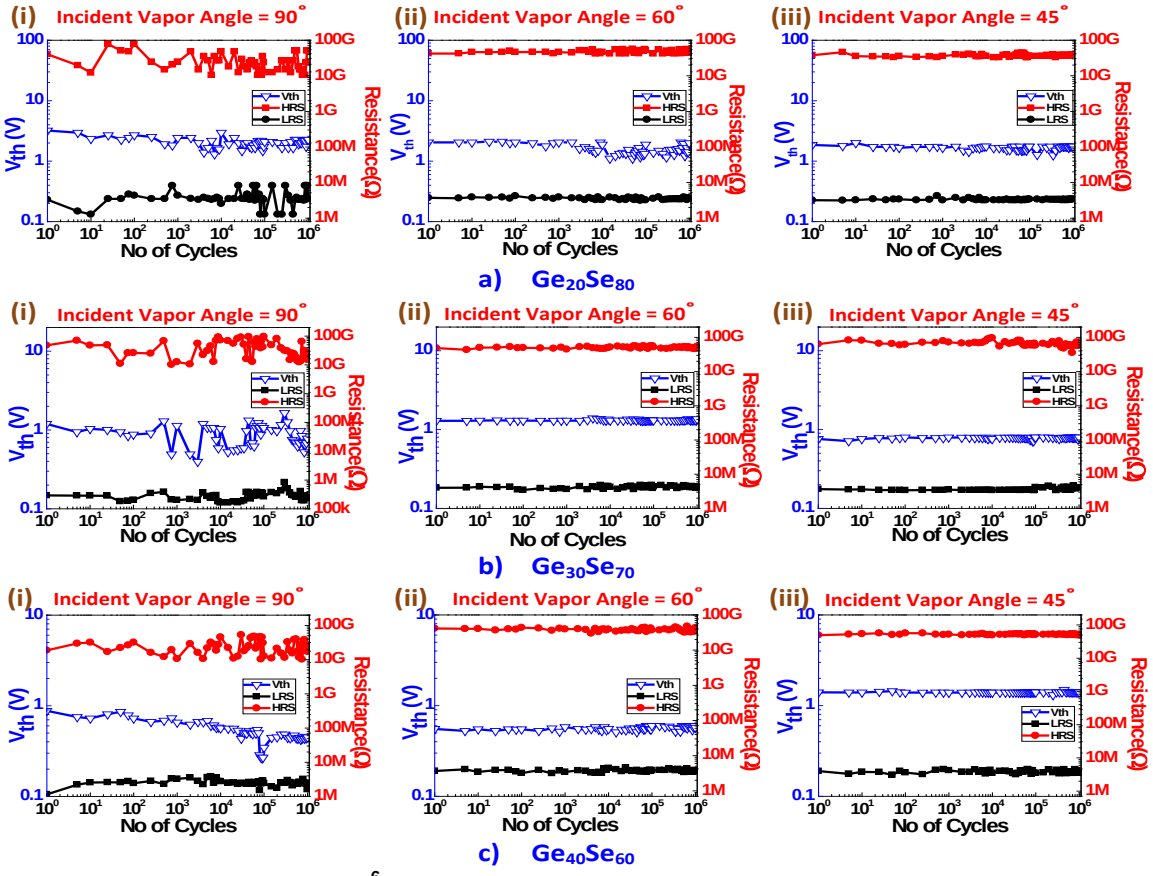

Figure 18 RV plot for 10^6 cycles of Ge-Se devices having nano-columnar structure in the active films under various incident angles: (i) α = 90°, (ii) α = 60°, (iii) α = 45°

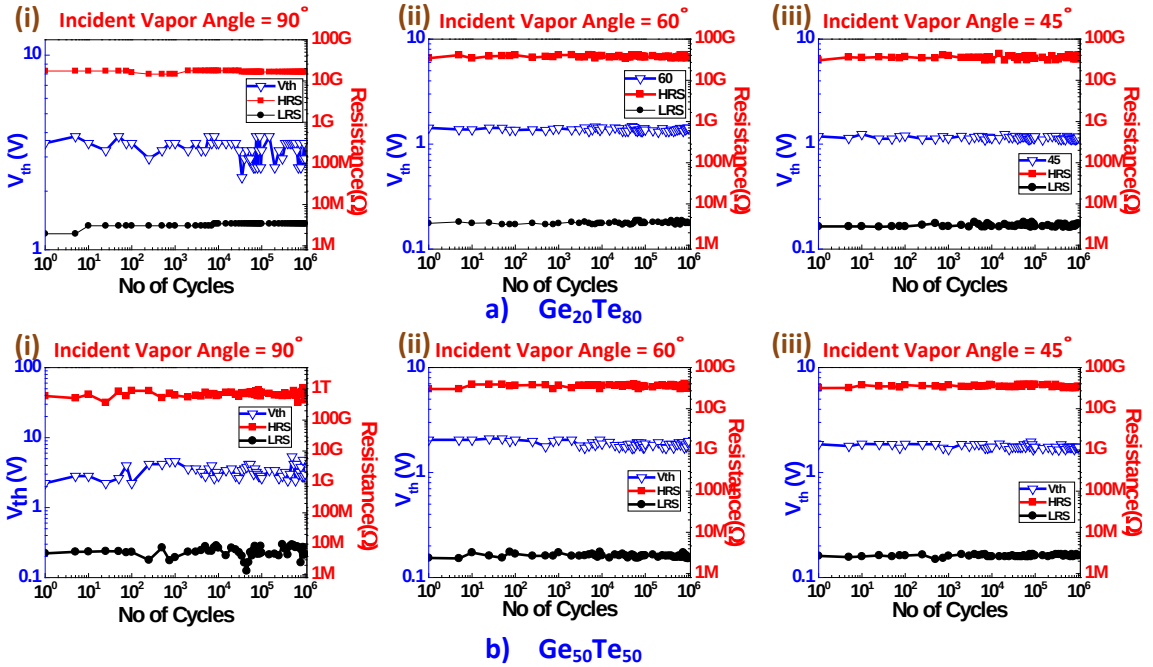

Figure 19 RV plot for 106 cycles of Ge-Te devices having nano-columnar structure in the active films under various incident angles: (i) α = 90°, (ii) α = 60°, (iii) α = 45°

Higher Temperature Measurements

In addition to the reliable device performance, the operating temperature range specified for existing memory technologies were investigated for the devices to be commercially viable. The fabricated RCBM devices were tested at 130°C which is well above the required specifications (95°C) of the developed memory technologies. The devices' memory window, in both the Ge-Se and Ge-Te system, did not show any degradation in performance as illustrated in Figure 20 and Figure 21. However, a slight change is observed in the switching threshold voltage at higher temperature compared to room temperature, which is attributed to thermal activation of the electrochemical process for filament formation.

Close observation of the high resistive state reveals a slight decrease in the state, which is in accordance with the expected behavior, i.e. increasing the temperature multiplies the number of charge carriers in a p-type semiconductor, thus enhancing the Ge-Se conductivity and therefore reducing the corresponding resistance. Despite of this reduction in the high resistive value, still more than four orders of magnitude difference is observed in the ON and OFF state of the devices. Hence, no additional temperature sensing circuitry is required to reduce the read out error.

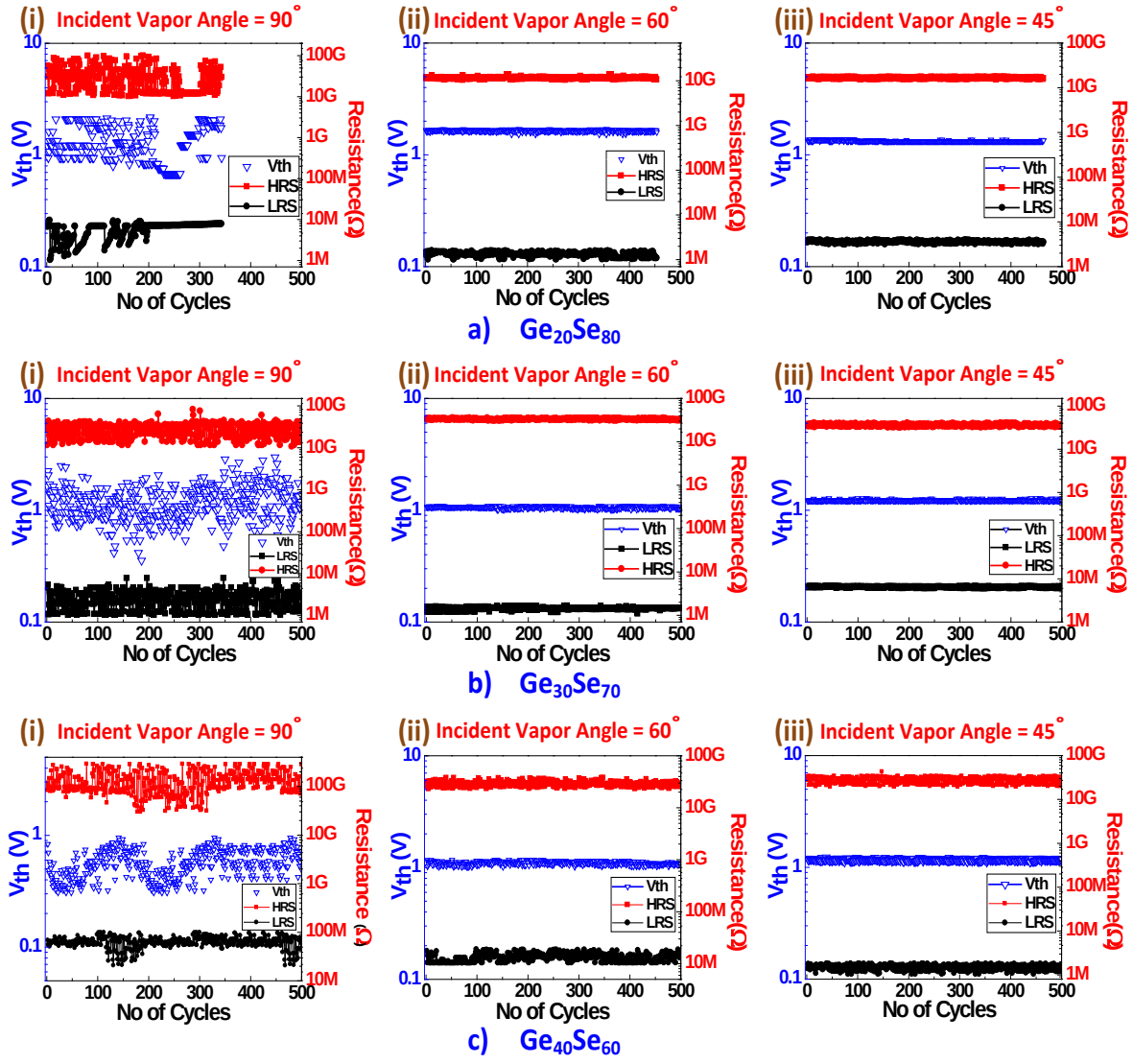

Figure 20 **500 cycles of RV plots for Ge-Se devices having nano-columnar structure**

in the active films under various incident angles: (i) α = 90°, (ii) α = 60°, (iii) α = 45°

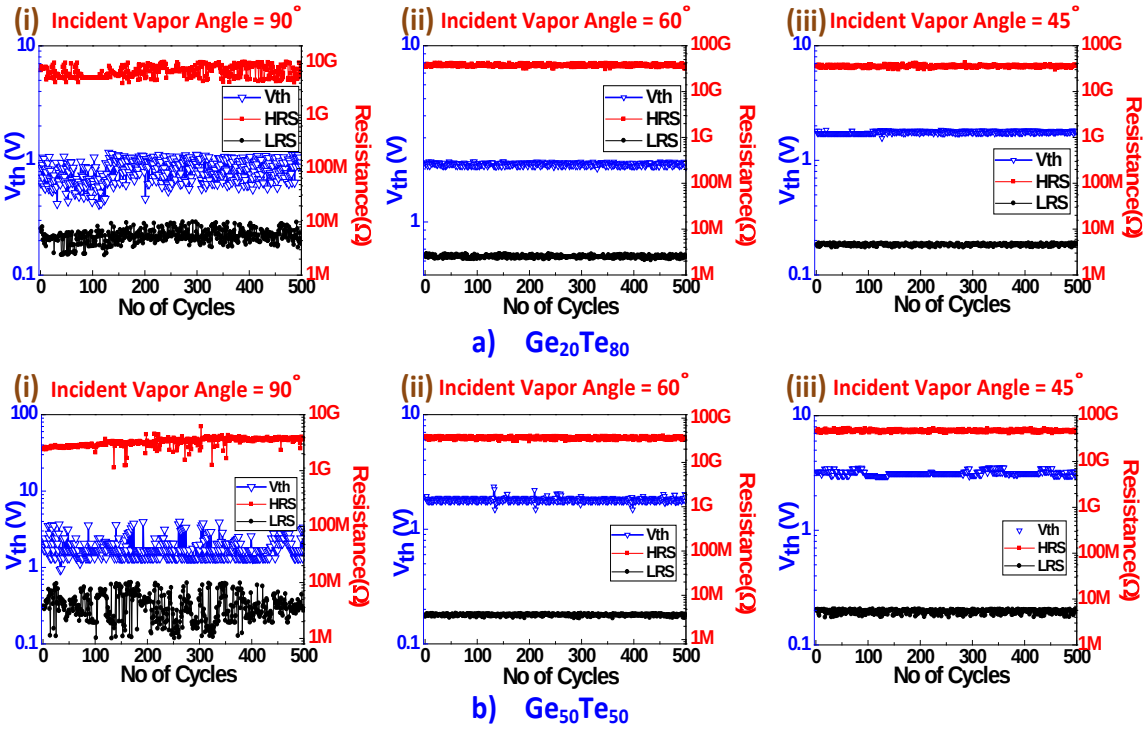

Figure 21 **500 cycles of RV plots for Ge-Te devices having nano-columnar structure in the active films under various incident angles: (i) α = 90°, (ii) α = 60°, (iii) α = 45°**

Retention Testing

The stability of the memory states of the fabricated column structured devices were analyzed through retention measurements. Once the devices were programmed, the change in state of the device would occur only when the conductive filament deteriorates over time. The fabricated devices were tested for retention properties at 90°C and 130°C to predict the device's lifetime. The state of the programmed devices was detected by reading the state of the cell with the parameter analyzer at specific times with a read voltage ranging from 0.3V to 0.5V. The retention testing results for the devices having nano-columnar structure are presented in Figure 22.

Since the high resistive state of the devices is above the resolution limit (10^{10} ohms), the devices were tested for their retention property in low resistive state only. The accelerated tested devices for retention properties can be interpolated with Arrhenius theory to predict the actual lifetime of the devices. The stable states achieved with the test results interpolates to over 11 years of data retention. Thus, the devices having the nano-columnar structure are well placed for being used in non-volatile applications.

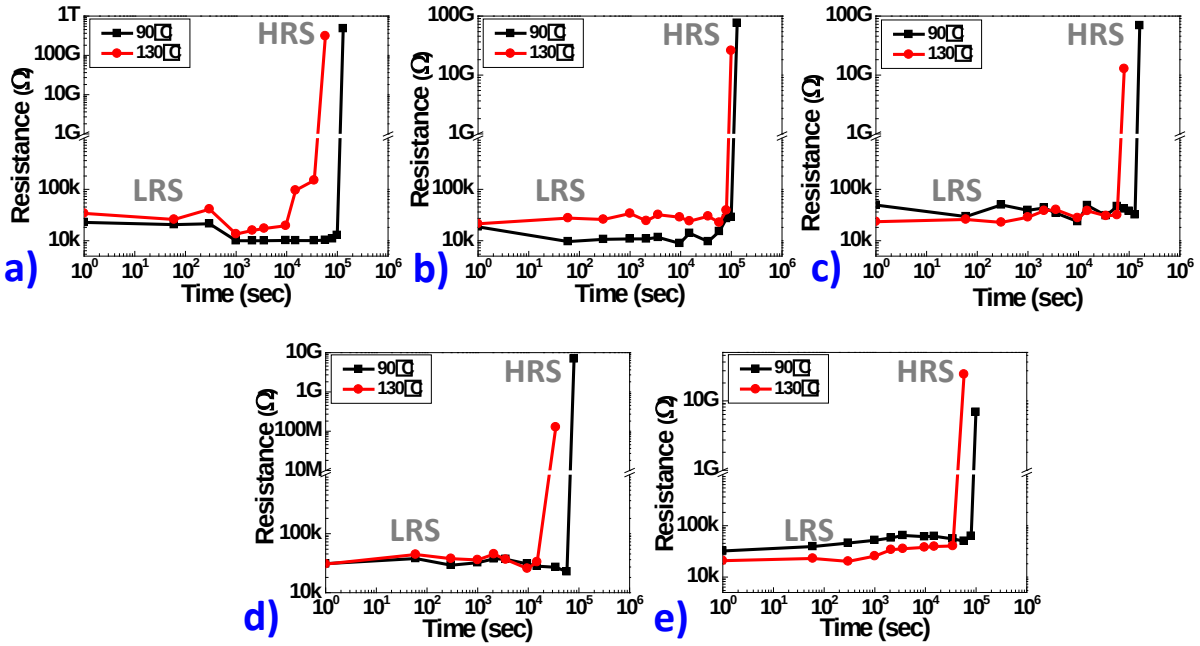

Figure 22 **Data retention of low resistive state of the devices written at a compliance current value of 10μA for (a) $Ge_{20}Se_{80}$ with α = 70°, (b) $Ge_{30}Se_{70}$ with α = 60°, (c) $Ge_{40}Se_{60}$ with α = 45°, (d) $Ge_{20}Te_{80}$ with α = 45°, and (e) $Ge_{50}Te_{50}$ with α = 30° devices. The data for the written bit is read at voltage ranging from 0.3V to 0.5V**

Multilevel Switching Capability

A memory cell that can be programmed to more than one state can store multiple bits, which will increase the storage density of the memory architecture. In RCBM technology, the ON state resistance (LRS) of the device can be programmed to multiple resistance levels. This can be achieved by controlling the write current (compliance current) through the cell being programmed.

To achieve multilevel switching in the fabricated nano-columnar structured devices, the RCBM cells were programmed with different write current levels controlled by the HP parametric analyzer. Since the voltage switching is achieved in all the studied Ge-Se and Ge-Te compositions under all the incident vapor angles, the same is achieved by setting multiple compliance current values to demonstrate multilevel switching. All the fabricated devices were tested with compliance current values separated by five orders of magnitude difference. The multilevel switching performance of $Ge_{30}Se_{70}$ nano-structured devices under vapor incident angle of 60° is demonstrated in Figure 23.

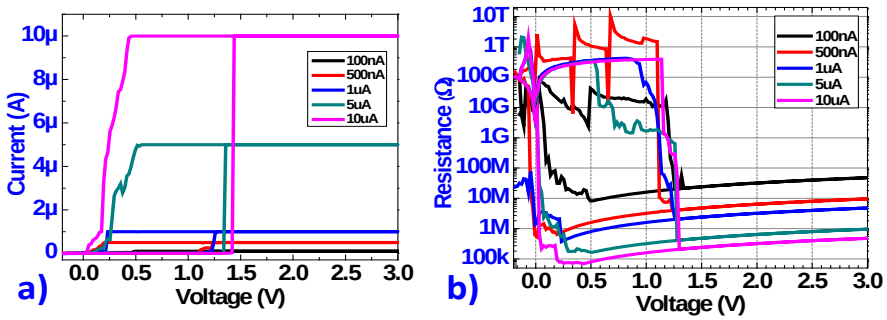

Figure 23 **(a) IV and (b) RV curves with varying compliance current values for $Ge_{30}Se_{70}$ column-structured devices with deposition angle, α = 60°**

The measured relation between the compliance current and the respective low resistant values is illustrated in Figure 6. A decrease in the low resistance value with increasing the compliance current can be observed. A change in the low resistance value from 5M to 500K is achievable by varying the compliance current from 100nA to 10µm. The presented data illustrate that the low resistance state of the RCBM cell can be programmed to different states by employing a defined compliance current level. This is the key advantage of resistive memory for competitiveness in the emerging memory technology.

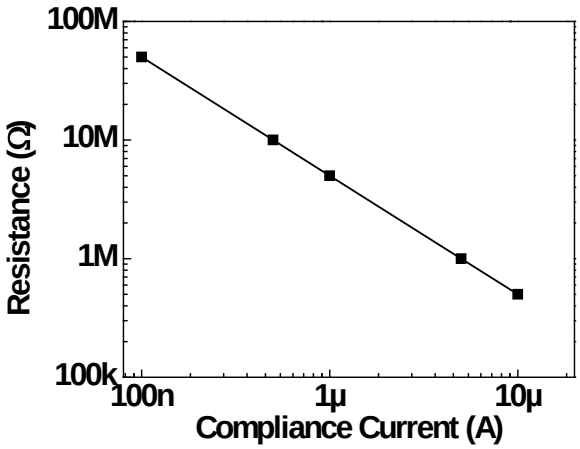

Figure 24 **Dependence of low resistive state on the compliance current value at room temperature**

Filament Growth through Columnar Structure - Atomic Level Switching

The environment within the SEM consists of high energy electron, which interacts with the filament. The random growth of the filament in normally deposited films and the interaction of the electrons in SEM will rupture the Ag filament as illustrated in Figure 25. This is a dynamic process that hinders the recording of the Ag filament, thus making SEM an unfavorable choice.

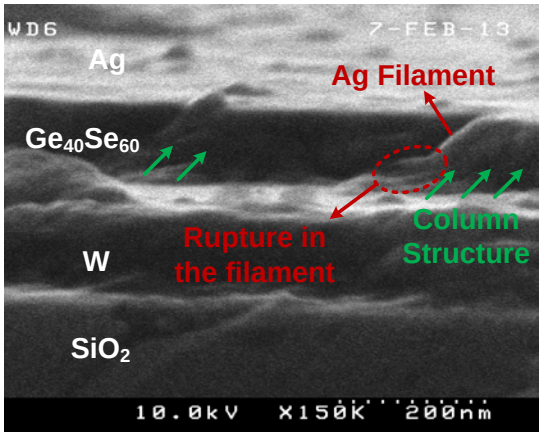

Figure 25 **SEM image of the filament rupture caused by electron beam**

To overcome this, and to illustrate the Ag diffusion and filament formation with no muti-branching through the pathways provided by columnar structure, a novel experimental setup for imaging the cross-sectional areas of the samples using AFM was engineered. These nano-electrical characterization techniques provided near atomic scale information on the fabricated devices, suggesting that these devices are scalable to atomic level.

The growth of the silver filament and intercalation of silver through the devices column structure, as a function of the applied voltage, was monitored and imaged using a Bruker Dimension Icon AFM operating in Bruker's proprietary PF-TUNA mode. Concurrent PF tapping and imaging, enabled identification of all the underlying films (SiO_2/W/ChG with nano-columnar structures/Ag) due to variations in topography and/or nano-mechanical properties of each film thus allowing to completely map the device structure using cross-sectional PF-TUNA imaging method.

The confirmation the silver filament growth through the inter-columnar spacing between the pillars is achieved by appropriately biasing the tip and stage. Since the tip was in contact with silver at the start of the scan, in order for the redox reaction to start, the tip was positively biased with respect to the stage. Figure 26 shows the growth of the silver filament (dark brown color) through the voids between the columns for the studied $Ge_{20}Se_{80}$, $Ge_{30}Se_{70}$, and $Ge_{40}Se_{60}$ devices with obliquely deposited active films. A close observation of the films reveals the formation of the filament with no multi-branching within the filament. A significant increase in the current can be observed in Figure 26a-c (vi-viii) due to the conduction path available between the tungsten and silver electrode.

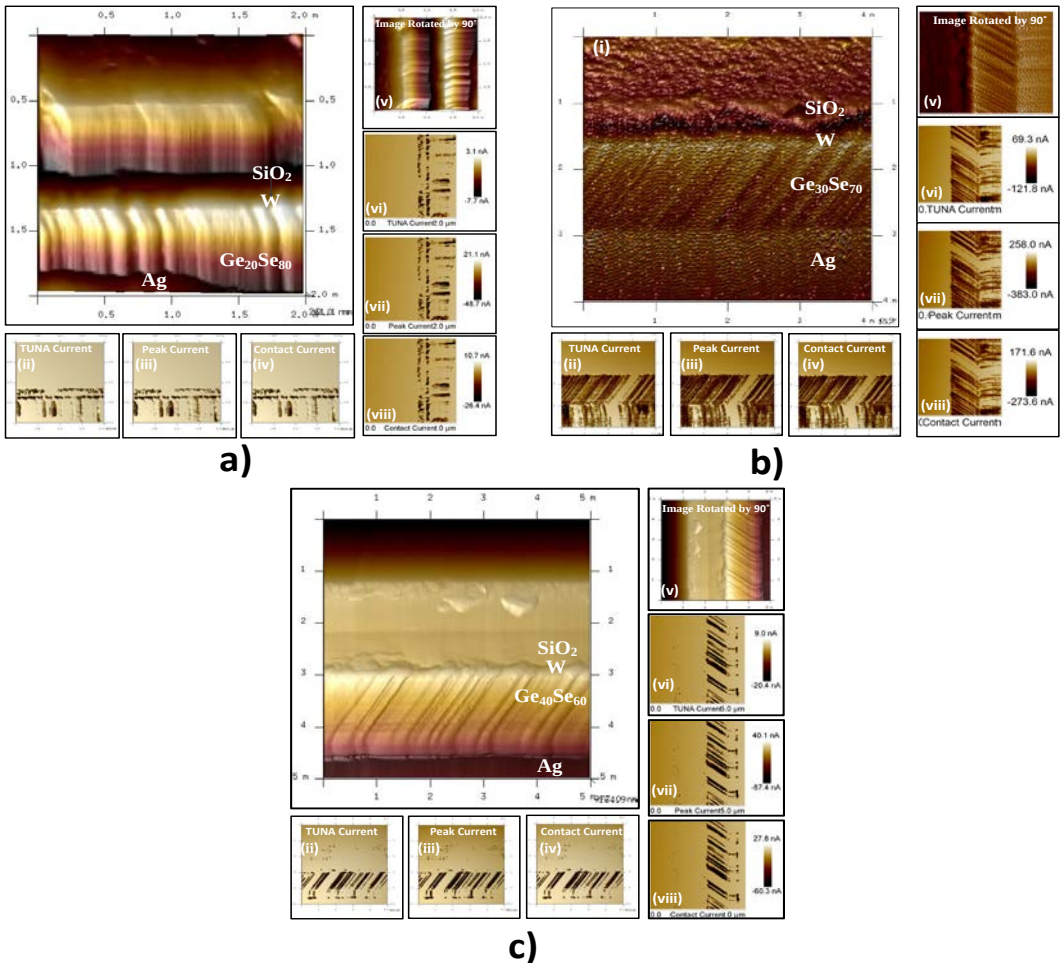

Figure 26 **PF-TUNA scans with stage biased at -0.5V and peak force set 10nN for (a) $Ge_{20}Se_{80}$ with α = 70°, (b) $Ge_{30}Se_{70}$ with α = 45°, and (c) $Ge_{40}Se_{60}$ with α = 30° where (i-iv) the top scan view and the filament growth through the voids in the columnar structure (v) the top view image rotated by 90° (vi-viii) the side scan view of the cross-sectional area and the filament growth through the voids in the columnar structure with corresponding current scale**

Apart from PF-TUNA measurements, PF-KPFM was also used to support the hypothesis that silver filament grows through the columnar structures. PF-KPFM measurements demonstrates a unique usefulness in characterizing the properties of various electronic devices by correlating the potential distribution within the device structure. The recorded KPFM data on $Ge_{30}Se_{70}$ films deposited at $\alpha = 45^{\circ}$ under unbiased and biased conditions is presented in Figure 27. A clear difference in the potential of the $Ge_{30}Se_{70}$ film can be observed under the two conditions. A close observation shows the formation of silver filament, after the bias was applied, through the columnar structure.

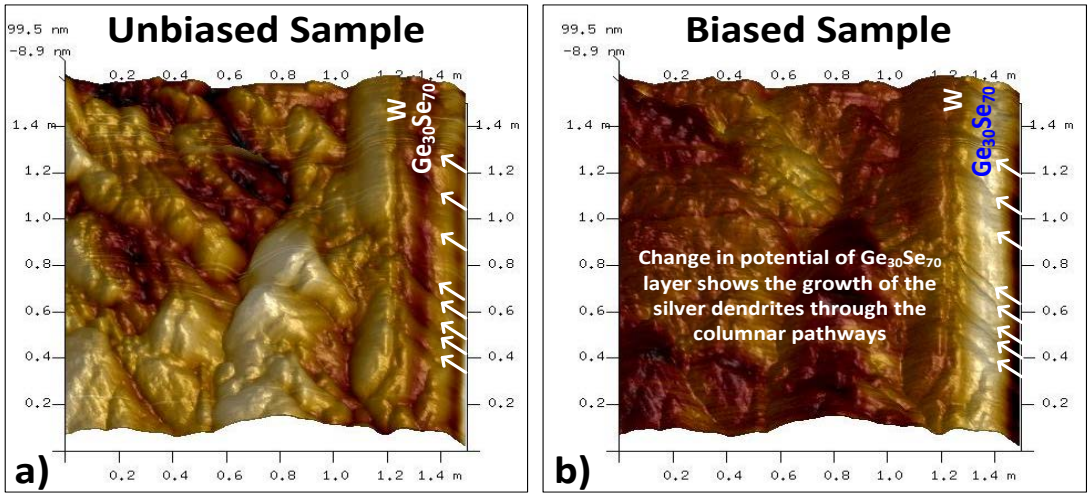

Figure 27 **PF-KPFM scan (a) under unbiased and (b) biased condition with peak force set to 10nN for $Ge_{30}Se_{70}$ film at $\alpha = 45^{\circ}$**

Conclusions

In this research work significant studies in materials engineering were made by creating nanostructure columnar rods in number of films with different composition. These advancements allowed the formation of filament growth within the nanostructure columnar rods, which considerably improved the performance of Redoxy Conductive Bridge Memory (RCBM) devices by solving the fundamental problem of multi-branching during the filament formation and growth. The particular findings of this research work, which represent the fulfillment of the milestones/ goals, depicted in the proposal are highlighted below:

- Nano-columnar structures in thin films were studied theoretically An empirical formula was suggested to predict the inclination of the column structures in chalcogenide glasses.

- Columnar structures were created in number of different films. They were characterized using a wide range of experimental techniques:
  - SEM and AFM tools were used to study the nano-columnar structures in thin films, which validated the presence of columnar structures in the Ge_xSe_{1-x} (x = 0.2, 0.3, 0.4) and Ge_xTe_{1-x} (x = 0.2, 0.5) chalcogenide glasses.
  - An increase in the surface roughness of the films was observed by decreasing the vapor flux angle, which suggested an increase in the inter-column voids.

- Raman results illustrated changes occurring in Ge-Se structure as a function of oblique angle deposition due to formation of a phase separated material or the relief of the packaging stress in the particular composition. Small alterations in chemical structure of the Ge-Te films were also detected due the presence of the rocksalt structure.

- Silver diffusion was studied and specific methods have been created to demonstrate the development of the diffusion process. They also proved that diffusion occurs only in the free channels formed in the structure of the hosting films.
- The electrical testing of the devices revealed Write/Read voltages were dependent on deposition angle. Due to this unique relationship of the devices, switching voltage can be engineered by varying the deposition angle.

- Formation of columnar structures enhanced the performance of devices fabricated with active films from all studied systems. These device exhibited excellent uniformity in switching voltage with endurance of well over 10^6 cycles, retention of over 10^4 seconds @ 130°C, and a good memory window.

- Nano-scaled electrical characterization of the devices through PF-TUNA and PF-KPFM illustrated the directional growth of the nano-ionic metallic filament through the nano-engineered columnar structures, with no multi-branching, which is the basis for the improved device performance.

The goal of this research work was to improve the RCBM device performance by providing new and innovative solutions for the active films. This was successfully achieved by formation of columnar structures that ensured single filament growth process. The processes, methodologies, and machines utilized in this work are currently available and being used by the major semiconductor companies, therefore these improved device performance can be replicated for mass device fabrication.

2. Describe the current state of the technology and related product/service: The production of Redoxy Conductive Bridge Memory (RCBM) devices is described in the International Technology Roadmap for Semiconductors (ITRS) as one of the most promising emerging technologies. The materials research related to these devices is predominantly related to experimenting with new materials but adjustment of some specific properties of the films as the suggested columnar structure which to restrict the development of the conductive filament in the devices have not been demonstrated yet.

3. List the number of faculty and student participants as a result of funding:
Dr. Maria Mitkova – faculty
Graduate Research Assistant: Muhammad Latif
Undergraduate Research Assistant: Tyler Nichol
Undergraduate Research Assistant: Brian Dambi
Undergraduate Research Assistant: Jasen Nielsen
Undergraduate Research Assistant: Corey Efaw

4. What are the potential economic benefits:

The introducing of the proposed technology in practice does not require any new type of equipment or additional investments. However the benefits which it will contribute to the devices performance will bring economic benefits coming from their improved reliability. Longer life and improved switching speed. Given that the number of these devices included in an integrated circuit could be very high, tis will multiply the benefits to a great extent.

5. Description future plans for project continuation or expansion:

The interest to the RCBM nonvolatile memory devices is very high and there are many studies related to them. However, in order these devices to be really useful, they have to be included in some integrated circuit. For them the most useful application is formation of memory arrays which to fulfil the needs of neuromorphic computing or other reconfigurable logic needs. For this we have ideas to develop new non-traditional, cheap and fast technologies for memory devices arrays formation. These technologies are not using the traditional photolithography which requires very expensive and sophisticated equipment. We will be very thankful if the State of Idaho Board of Education continues with funding of such project in order to be able to make the next step in development of new progressive technologies in the field of neural networks and reconfigurable logic.

6. Please provide a final expenditure report (attached) and include any comments here:

FINAL EXPENDITURE REPORT

A. FACULTY AND STAFF		
Name/Title	$ Amount Requested	Actual $ Spent
Maria Mitkova	$10,028	$10,028
B. VISITING PROFESSORS		
Name/Title	$ Amount Requested	Actual $ Spent
C. POST DOCTORAL ASSOCIATES/OTHER PROFESSIONALS		
Name/Title	$ Amount Requested	Actual $ Spent
D. GRADUATE/UNDERGRADUATE STUDENTS		
Name/Title	$ Amount Requested	Actual $ Spent
Graduate Research Assistant: Muhammad Latif	$12,000	$9,692.34
Undergraduate Research Assistant: Tyler Nichol	$5,550	$6,693.03
Undergraduate Research Assistant: Brian Dambi		$805.00
Undergraduate Research Assistant: Jasen Nielsen		$1676.38
Undergraduate Research Assistant: Corey Efaw		$609.25
E. FRINGE BENEFITS		
Rate of Fringe (%)	$ Amount Requested	Actual $ Spent
Maria Mitkva	$3,109	$2,466.99

Muhammad Latif	$120	$61.69
Tyler Nichol	$56	$54.46
Brian Dambi		$3.60
Jasen Nielsen		$5.33
Corey Efaw		$10.95
PERSONNEL SUBTOTAL:	**$30,862.00**	**$32.107.02**

F. EQUIPMENT: (List each item with a cost in excess of $1000)

Item/Description	$ Amount Requested	Actual $ Spent
1.		
2.		
EQUIPMENT SUBTOTAL:		$0.00

G. TRAVEL

Description	$ Amount Requested	Actual $ Spent
1.Tyler Nichol/ Muhammad Latif MRS Spring Conference	$3,828	$2,170.92
2. Maria Mitkova Travel to Arizona in November		$578.27
3.Maria Mitkova Travel to Arizona in February		$760.38
TRAVEL SUBTOTAL:	$3,828	$3,509.57

H. PARTICIPANT SUPPORT COSTS:

Description	$ Amount Requested	Actual $ Spent
1.Muhammad Latif Student Fees	$4,760	$2,870.00
2.		
3		
PARTICIPANT SUPPORT COSTS SUBTOTAL:	$4,760	$2,870.00

I. OTHER DIRECT COSTS:

Description		$ Amount Requested	Actual $ Spent
1.Recharge Cost (IML/BSCMC)		$3,300	$3,100.00
2 Supplies.		$3,000	$4,163.41
3.			
OTHER DIRECT COSTS SUBTOTAL:		$6,300	$7,263.41

TOTAL COSTS (Add Subtotals):	$45,750	$45,750
TOTAL AMOUNT REQUESTED:		$45,750
TOTAL AMOUNT SPENT:		$45,750

7. List invention disclosures, patent, copyright and PVP applications filed, technology licenses/options signed, start-up businesses created, and industry involvement:

   1) Structured Chalcogenide Glass Films for Redox Conductive Bridge Nonvolatile Memristors (BSU FIle #132, patent app. 61/823,783)

2) Structured Oxide Films for Redox Conductive Bridge Nonvolatile Memristors, (BSU File # 141, patent app. 61/847,974)

8. Any other pertinent information:

The most recent requirements of the International Roadmap for Semiconductors (ITRS) brings the problems on which the reported project is based as well our proposal for its further development as a specific requirements of the industry in the next five years:

- Bridge the gap that exists between materials behaviors and device functions.
- Accommodate the heterogeneous integration of dissimilar materials
- Reliability issues should be identified & addressed early in the technology development

  http://www.itrs.net/Links/2013ITRS/2013TableSummaries/2013ERD_SummaryTable.pdf

This edifies the importance and the benefits form the further development, as proposed by us of the project a subject of this report.